出國報告（出國類別：研習會）

南海非線性內孤立波之研究

服務機關：海軍軍官學校

姓名職稱：楊穎堅

派赴國家：奧地利

報告日期：99 年 7 月 22 日

出國時間：99 年 4 月 30 日－99 年 5 月 10 日

目次

摘要

於 99 年 4 月 30 日至 5 月 10 日期間，前往奧地利維也納市參加歐洲地球科學聯盟(European G eosciences U nion)舉辦之 2010 年聯合會(General A ssembly 2010)，吸收最新之地球科學研究成果，並發表國科會專題研究計畫之內波研究成果，論文名稱為：Convex and concave types of mode-2 internal solitary waves。

Two types of second baroclinic mode (mode-2) internal solitary waves (ISWs) were found in the continental slope of the northern South China Sea. One has waveform with upward/downward and downward/upward displacement of isotherm in the upper and lower water columns, respectively. It is a typical type of mode-2 ISW and named as convex wave. Another, named as concave wave, has waveform with reverse vertical displacement of isotherm. Few concave waves observed in the South China Sea. It is the first time documented here.

Based on the K-dV equation, an analytical three-layer ocean model is used to study the characters of two types of mode-2 ISW. The analytical solution is primarily a function of the thickness of each layer and the density difference between the layers. The thickness of middle layer plays a significant role on the resulted mode-2 ISW. The convex wave could be generated as the thickness of middle layer is relatively thinner than the upper and lower layers. Whereas the thickness of middle layer is larger than half of the water depth, only the concave wave could be produced. In accordance with K-dV equation, the positive and negative quadratic nonlinear coefficient, alpha2, which is also primarily dominated by the thickness of middle layer, leads the convex and concave waves, respectively.

The analytical solution shows that the wave propagation of the convex (concave) wave has the same direction of current velocity in middle (upper or lower) layer.

The analysis three-layer model properly reproduces the characteristics of observed mode-2 ISW in the South China Sea. It also provides a criterion for the existence of convex and concave wave. Since a stratified ocean with a thick middle layer is rare, the concave wave was seldom seen. This inference agrees with our observation.

出席國際會議心得報告

1 目的：

與國際著名學者討論南海的非線性內波並發表個人論文。

2 過程：

主持人於 2010 年 4 月 30 日晚上由桃園國際機場出關前往奧地利維也納市，於隔日(5 月 1 日，週六)上午到達目的地後即稍作休息。2~7 日參加演討會，並於 5 月 7 日上午發表論文，論文題目為 Convex and concave types of mode-2 internal solitary waves，內容主要敘述在南海北部陸棚邊緣的第二模態內孤立波的有兩種型態，分別是 Convex 與 Concave，並以三層海洋結構，探討其型態與水層厚度之關聯。發表期間，曾與一些相關的研究人員進行討論，如俄羅斯科學院應用物理研究所的 Dr. Tatiana Talipova 等國際著名之內波研究學者等，一起討論南海的非線性內波及我的論文研究成果，以及討論未來共同合作研究的可行性。研討會於 5 月 7 日傍晚結束，5 月 8 日(週六)等待飛機，5 月 9 日(周日)早上，主持人搭上飛機返國，於 5 月 10 日早上返抵國門。

3 心得：

3.1 在發表論文"Convex and concave types of mode-2 internal solitary waves"期間，敘述少見的第二模態內孤立波的兩種波形，討論熱烈，收穫良多。期間有些學者建議將其發表於 SCI 期刊。主持人返國後，即與其他共同作者討論，並彙整議場意見，撰寫成期刊論文，目前已投稿至 Journal of Physical Oceanography (SCI)期刊。

3.2 會議期間與各研究人員討論南海的內波特性，有位國際知名的內波研究學者 Dr. Andrey Serebryany，他是從事內波的電腦數值模擬，他將於今年暑假拜訪台灣，屆時他希望能與台灣的內波研究人員會面，進行更深入的討論與共同研究。

4：建議事項：

此次讓個人受益良多，建議可多鼓勵國內學者至國外研習。

附錄一：論文

Convex and Concave Types of Second Baroclinic Mode Internal Solitary Waves

Yiing Jang Yang[1], Ying Chih Fang[2], Tswen Yung Tang[2,*], and Steven R. Ramp[3]

[1]*Department of Marine Science, Naval Academy, Kaohsiung, Taiwan*

[2]*Institute of Oceanography, National Taiwan University, Taipei, Taiwan*

[3]*Monterey Bay Aquarium Research Institute, Moss Landing, California, USA*

[*]*Corresponding author address*: Tswen Yung Tang, Institute of Oceanography, National Taiwan University, No 1, Section 4, Roosevelt Road, Taipei 106, Taiwan.

E-mail: tyt@ntu.edu.tw

Abstract

Two types of second baroclinic mode (mode-2) internal solitary waves (ISWs) were found on the continental slope of the northern South China Sea. The convex waveform displaced the thermal structure upwards in the upper layer and downwards in the lower layer causing a bulge in the thermocline. The concave waveform did the opposite, causing a constriction. A few concave waves were observed in the South China Sea, marking the first documentation of such waves. On the basis of the Korteweg-de Vries (K-dV) equation, an analytical three-layer ocean model was used to study the characteristics of the two mode-2 ISW types. The analytical solution was primarily a function of the thickness of each layer and the density difference between the layers. Middle layer thickness plays a key role in the resulting mode-2 ISW. A convex wave was generated when the middle layer thickness was relatively thinner than the upper and lower layers, whereas only a concave wave could be produced when the middle layer thickness was larger than half the water depth. In accordance with the K-dV equation, a positive and negative quadratic nonlinearity coefficient, α_2, which is primarily dominated by the middle layer thickness, resulted in convex and concave waves, respectively. The analytical solution showed that the wave propagation of a convex (concave) wave has the same direction as the current velocity in the middle (upper or

lower) layer. The three-layer ocean model analysis properly reproduced the characteristics of the observed mode-2 ISWs in the South China Sea and provided a criterion for the existence of convex or concave waves. Concave waves were seldom seen because of the rarity of a stratified ocean with a thick middle layer. This analytical result agreed well with the observations.

1. Introduction

An internal solitary wave (ISW) is a commonly observed phenomenon in many of the world's stratified oceans. Its prevalent form is the first baroclinic mode (mode-1) ISW. A mode-1 ISW produces strong vertical mixing and can impact underwater vessels or structures. Mode-1 ISWs have been widely investigated through theoretical, modeling, and observational efforts (Helfrich and Melville 2006; Apel et al. 2007).

The second baroclinic mode (mode-2) ISW is much less common than the mode-1 wave and has only occasionally been observed. Theoretically, a mode-2 ISW should take on one of two types of waveforms: In the upper layer, a "convex wave" has a leading upward displacement of an isotherm ahead of the wave and a trailing downward displacement behind it. Deeper in the water column, the opposite is true, causing it to be described as a bulge-shape, double-hump, varicose, or sausage-type wave (Davis and Acrivos 1967; Stamp and Jacka 1995; Ostrovsky and Stepanyants 2005; Moum et al. 2008). Pioneering investigations, including theoretical investigations, have all described this type of wave (Benjamin 1967; Davis and Acrivos 1967; Akylas and Grimshaw 1992; Vlasenko 1994; Grimshaw 1997), laboratory experiments (Davis and Acrivos 1967; Kao and Pao 1980; Maxworthy 1980; Honji et al. 1995; Stamp and Jacka 1995; Vlasenko and Hutter 2001; Mehta et al. 2002; Sutherland 2002), numerical analyses (Tung et al. 1982;

Terez and Knio 1998; Rubino et al. 2001; Vlasenko and Hutter 2001; Rusås and Grue 2002; Stastna and Peltier 2005; Vlasenko and Alpers 2005), and field observations (Farmer and Smith 1980; Konyaev et al. 1995; Saggio and Imberger 1998, 2001; Antenucci et al. 2000; Boegman et al. 2003; Duda et al. 2004; Yang et al. 2004; Bougucki et al. 2005; Sabinin and Serebryany 2005; Moum et al. 2008; Shroyer et al. 2010).

Theoretically, however, a second type of mode-2 wave is possible. Sometimes called "reverse convex" waves, these waves will be referred to here as "concave" waves and have the opposite character from convex waves. The concave waves have an hourglass-shaped constriction of the thermal structure with a downward followed by an upward deflection of the thermal structure in the upper layer associated with the opposite condition in the lower layer.

A long-term current velocity and temperature mooring was deployed on the continental slope of the northern South China Sea (Fig. 1) under the joint research program known as Variations Around the Northern South China Sea (VANS, supported by Taiwan) and the Windy Islands Soliton Experiment (WISE, supported by the U.S.). The observed current velocity and temperature revealed that mode-2 ISWs were active, and both convex and concave waves were found. The project identified 78 convex waves (Yang et al. 2009) and four concave waves, marking the first time concave waves have been observed in nature.

This article describes the characteristics of two distinct types of mode-2 ISWs on the continental slope of the northern South China Sea and discusses how stratification affects their formation. Furthermore, an analytical three-layer ocean model was used to study and interpret the observed convex and concave waves. The remainder of this paper is organized as follows. Section 2 describes the observational results of the convex and concave waves. The analytical interpretations applied for mode-2 ISWs under a three-layer ocean model are presented, and the results are shown in Sections 3 and 4, respectively. Finally, Section 5 provides a discussion of the two mode-2 ISW types.

2. Observations

The current velocity and temperature mooring was deployed at a depth of 350 m from 29 April to 28 July 2005 and from 2 November 2005 to 24 February 2006. A 300 kHz self-contained acoustic Doppler current profiler (ADCP) was mounted at 100 m and measured the current velocity from 15 to 95 m in 4-m bins and recorded the temperature at 100 m. The ping rate was 1 s, and the averaging and recording interval was 1 min. Temperature was recorded every minute. Three ducted paddlewheel recording current meters (RCM8s) were located at 160, 220, and 310 m. The RCM8s recorded the current velocity and temperature every 5 min. The mooring had 16 temperature recorders [one ADCP, three RCM8s, seven temperature-pressure recorders (TPs), four conductivity-temperature-depth sensors (CTDs), and one temperature recorder (T-pod)] spanning from 32 m to 338 m. The TPs and T-pod sampled every minute, and the CTDs sampled every 2 min.

Because the passage of ISWs would induce a temperature perturbation, a time series of temperature measurements was used to identify mode-2 ISW episodes. In a convex wave, the temperature theoretically undergoes a decreasing and then an increasing temperature evolution in the upper layer and the opposite temperature evolution in the lower layer. A concave wave has reverse temperature evolutions; therefore, for convex and concave waves, the isotherm contour plot would reveal a "double-hump" like and a "reverse double-hump" like waveform, respectively. Whether the wave was convex or concave could be determined by the thermal displacement pattern. During the observation period, 78 convex waves and four concave waves were identified.

Current velocity was also used to further confirm the mode-2 ISW episode. Theoretically, the mode-2 ISW current velocity has a three-layered structure with two vertical nodal points (zero-crossing points). The velocities of the upper and lower layers are in the same direction but opposite to the velocity in the middle layer. The convex wave propagation direction is consistent with the current direction in the middle layer. The propagation direction of a concave wave is unknown, and the relationship between current distribution and propagation direction has not been studied. For each mode-2 ISW episode, the horizontal current velocity perturbation, which could be associated with the mode-2 ISW, was calculated by subtracting the background current velocity from the measured current velocity. The background current was defined as the average current 30 min before the episode.

The vertical velocity perturbation (w') of whole water column associated with mode-2 ISWs, was estimated from the wave temperature perturbation using the temperature conservation equation with the assumption of negligible horizontal advection and heat conduction:

$$w'(z,t) \approx -\frac{\dfrac{T^h(z,t+\Delta t)-T^h(z,t)}{\Delta t}}{\dfrac{T^b(z+\Delta z,t)-T^b(z,t)}{\Delta z}}, \tag{1}$$

where $T^h(z,t)$ is the 5-hr high-pass-filtered temperature, $T^b(z,t)$ is the 36-hr low-pass-filtered temperature, z is the depth where the temperature sensor was mounted, Δz is the depth difference between the two temperature sensors, t is the time when the mode-2 ISW passed the mooring, and Δt is 1 min. Theoretically, w' has a two-layered structure with one nodal point vertically and has opposite directions in the upper and lower layers, respectively. In the upper layer, w' is positive and then negative (upwelling/downwelling) for convex waves and negative and then positive (downwelling/upwelling) for concave waves. The values of w' computed in this way agreed well with the ADCP observations where available (in the upper water column < 100 m depth).

In the following paragraphs, a convex wave and a concave wave are used as examples to illustrate their characteristics.

2.1 Convex waves

The characteristics of convex waves such as amplitude, time scale, characteristic width, and phase speed have been reported by Yang et al. (2009). A typical isotherm contour (Fig. 2a) behaved like a “double-hump” waveform from 23:20 to 24:00 GMT 27 June 2005, indicating a convex wave. Figure 2b shows the perturbation of the eastward velocity component (u'). The u' induced by the convex wave had an eastward acceleration and then a deceleration evolution above 60 m and at 220 m and 310 m, and the opposite pattern between 60 m and 100 m and at 160 m. This result implies that there were two u' nodal points: one at approximately 60 m and another between 160 m and 220 m. The perturbation of the northward velocity component (v', not shown) had an evolution similar to u', whereas the v' amplitude was much smaller than that of u'. Therefore, the primary propagation direction of this convex wave was westward, consistent with mode-1 waves observed in the area (Ramp et al. 2010). The corresponding depths of the local maximum and minimum w' were near 80 m and 200 m, respectively (Fig. 2c). The positions of the local maximum/minimum w' were close to the positions of the two u' nodal points.

2.2 Concave waves

An example of a concave wave is shown in Fig. 3. The thermal displacement pattern (Fig. 3a) of the concave wave was opposite that of the convex wave. The vertical isotherm displacements at 24°C and 15°C were approximately -20 m and 40 m, respectively. The isotherms showed a downward and then an upward displacement above 140 m and the opposite evolution below, in which a “reverse double-hump” waveform evolved in the isotherm depth contour. Similar to the previous convex wave, the v' amplitude was relatively smaller than that of u'; hence we only consider u' here. Figure 3b demonstrates how u' was induced by the concave wave. At 23:10

GMT 9 July 2005, a negative u' was found above 30 m, whereas a positive u' was found below. The u' nodal point was identified near 30 m. The RCM8s at 160 m and 220 m also experienced a positive u' between 30 m and 220 m, whereas the RCM8 at 310 m experienced a negative u'. This result shows that another u' nodal point was located between 220 and 310 m. The vertical velocity component, w', also revealed a clear modal structure (Fig. 3c). At 23:05 GMT 9 July 2005, a downwelling occurred above 140 m, whereas an upwelling occurred below. Consequently, the w' nodal point was near 140 m. The perturbation induced by the concave wave was a downwelling/upwelling process above and below the w' nodal point. The corresponding depths of the local maximum and minimum w' were near 30 m and 240 m, respectively. The positions of the local maximum/minimum w' were also in accordance with the positions of the two u' nodal points.

Only four concave waves were found. The average amplitude of the upper part of the wave was 15 ± 4.3 m, while it was 27 ± 12.1 m for the lower part. The average time duration was 29 ± 4.9 min.

Yih (1960) inferred that a three-layer fluid system could have mode-2 waves. Actually, a nearly three-layer density structure has been observed in the northern South China Sea (Yang et al. 2004). Therefore, an analytic three-layer ocean model was established to study the characteristics of convex and concave waves.

3. Analytic three-layer ocean model

The vertical velocity structure function, W_n, is governed by the Taylor-Goldstein equation to consider the hydrostatic, frictionless internal motion without background current and to satisfy the Boussinesq approximation (Gill 1982):

$$\frac{d^2 W_n(z)}{dz^2} + \frac{N^2(z)}{c_n^2} W_n(z) = 0, \tag{2}$$

where $W_n(z)$ is the eigenfunction (or vertical structure function) for the *n*th mode, c_n is the eigenvalue (or modal phase velocity of the linear wave), and $N(z)$ is the Brunt-Väisälä (or buoyancy) frequency. The vertical modes of horizontal $U_n(z)$ and vertical motion are related by $U_n(z) = dW_n(z)/dz$. The theoretical vertical structures can be calculated by the buoyancy frequency profile.

For the simplified case of a three-layer ocean (Fig. 4a), the thicknesses corresponding to the upper, middle, and lower layers are h_1, h_2, and h_3, respectively. The densities corresponding to the upper, middle, and lower layers are $\rho_0 - \Delta\rho_1$, ρ_0, and $\rho_0 + \Delta\rho_2$, respectively, where $0 < \Delta\rho_1, \Delta\rho_2 << \rho_0$. $N(z) = 0$ except at two interfaces, $N(-h_1)=\sqrt{g'_1/\Delta z}$ and $N(-h_1-h_2)=\sqrt{g'_2/\Delta z}$, where g'_1 and g'_2 are $\Delta\rho_1 g/\rho_0$ and $\Delta\rho_2 g/\rho_0$, respectively, g is gravitational acceleration, and Δz is a small value variable.

Imposed on the rigid-lid boundary condition, $W_n(0)=0$ and $W_n(-h_1-h_2-h_3)=0$, the analytical solutions for Eq. (2) are as follows:

$$W_n(z)=\begin{cases}-\dfrac{z}{h_1} & -h_1\le z\le 0\\ \dfrac{1-\gamma_n}{h_2}(z+h_1+h_2)+\gamma_n & -h_1-h_2\le z\le -h_1\\ \dfrac{\gamma_n}{h_3}(z+h_1+h_2+h_3) & -h_1-h_2-h_3\le z\le -h_1-h_2\end{cases} \tag{3}$$

$$U_n(z)=\begin{cases}-\dfrac{1}{h_1} & -h_1\le z\le 0\\ \dfrac{1-\gamma_n}{h_2} & -h_1-h_2\le z\le -h_1\\ \dfrac{\gamma_n}{h_3} & -h_1-h_2-h_3\le z\le -h_1-h_2\end{cases} \tag{4}$$

where γ_n is the ratio of the vertical velocity component at the lower interface to that at the upper interface: $W_n(-h_1-h_2)/W_n(-h_1)$. Integrating Eq. (2) from $-h_1-\Delta z/2$ to $-h_1+\Delta z/2$ and from $-h_1-h_2-\Delta z/2$ to $-h_1-h_2+\Delta z/2$, γ_n can be expressed as follows:

$$\gamma_n = -\left(\frac{h_2 g'_1}{c_n^2} - \frac{h_2}{h_1} - 1\right) \tag{5}$$

$$\gamma_n = -\left(\frac{h_2 g'_2}{c_n^2} - \frac{h_2}{h_3} - 1\right)^{-1} \tag{6}$$

Substituting γ_n of Eq. (6) into Eq. (5), a single phase velocity equation c_n is obtained:

$$(h_1 + h_2 + h_3)c_n^4 - [h_1(h_2 + h_3)g'_1 + (h_1 + h_2)h_3 g'_2]c_n^2 + h_1 h_2 h_3 g'_1 g'_2 = 0 \tag{7}$$

Therefore, the eigenvalues (or linear internal wave modal phase speed) of the Taylor-Goldstein equation, c_1 and c_2, are as follows:

$$c_1^2 = \frac{h_1(h_2 + h_3)g'_1 + (h_1 + h_2)h_3 g'_2}{2(h_1 + h_2 + h_3)} + \frac{\sqrt{(h_1(h_2 + h_3)g'_1 + (h_1 + h_2)h_3 g'_2)^2 - 4(h_1 + h_2 + h_3)h_1 h_2 h_3 g'_1 g'_2}}{2(h_1 + h_2 + h_3)} \tag{8}$$

$$c_2^2 = \frac{h_1(h_2 + h_3)g'_1 + (h_1 + h_2)h_3 g'_2}{2(h_1 + h_2 + h_3)} - \frac{\sqrt{(h_1(h_2 + h_3)g'_1 + (h_1 + h_2)h_3 g'_2)^2 - 4(h_1 + h_2 + h_3)h_1 h_2 h_3 g'_1 g'_2}}{2(h_1 + h_2 + h_3)} \tag{9}$$

where c_1 and c_2, which have similar formulations derived by Grimshaw et al. (1997) and Rubino et al. (2001), represent the phase speed of faster (mode-1) and slower (mode-2) mode linear internal waves, respectively. If there is no density difference at either the upper ($\Delta\rho_1 = 0, \Delta\rho_2 \neq 0$) or lower ($\Delta\rho_1 \neq 0, \Delta\rho_2 = 0$) interfaces, the three-layer ocean model degenerates into a two-layer ocean model and only mode-1 motion remains such that $c_2 = 0$ and $c_1 = \sqrt{h_1(h_2+h_3)g'_1/(h_1+(h_2+h_3))}$ or $c_1 = \sqrt{(h_1+h_2)h_3 g'_2/((h_1+h_2)+h_3)}$, respectively.

From Eqs. (5) and (6), we can obtain the relationship between γ_1 and γ_2: $\gamma_1 - \gamma_2 = (c_2^{-2} - c_1^{-2})h_2 g'_1 > 0$ and $\gamma_1\gamma_2 = -g'_1/g'_2 < 0$. Thus, $\gamma_1 > 0$ and $\gamma_2 < 0$. For $n = 1$, the mode-1 motion accompanies faster phase speed (c_1) and in-phase vertical motion at the upper and lower interfaces ($\gamma_1 > 0$). However, if $n = 2$, the mode-2 motion accompanies the slower phase speed (c_2) and out-of-phase vertical motion at the upper and lower interfaces ($\gamma_2 < 0$). The second mode eigenfunctions of the Taylor-Goldstein equation, $U_2(z)$ and $W_2(z)$, are shown in Figs. 4b and 4c, respectively.

According to Benney (1966), Lee and Beardsley (1974), Pelinovsky and Shavratsky (1977), Maslowe and Redekopp (1980), Grimshaw (1981), Gear and Grimshaw (1983), Apel et al. (1997), and Apel (2003), the modal displacement η_n is governed by the

Korteweg-de Vries (K-dV) equation neglecting rotational effects and energy exchange between modes and assuming weakly nonlinear finite-amplitude plane progressive waves propagating in a specific direction (Korteweg and de Vries 1895):

$$\frac{\partial \eta_n}{\partial t} + c_n \frac{\partial \eta_n}{\partial x} + \alpha_n \eta_n \frac{\partial \eta_n}{\partial x} + \beta_n \frac{\partial^3 \eta_n}{\partial x^3} = 0, \tag{10}$$

where x is the wave front propagation direction and α_n and β_n are the quadratic nonlinear and dispersive coefficients for the *n*th mode, respectively. Both coefficients are also called "environmental parameters," as they account for conditions such as stratification (or Taylor-Goldstein equation eigenfunctions) and water depth (H) without background current as follows (Lee and Beardsley 1974):

$$\alpha_n = \frac{3c_n}{2} \frac{\int_{-H}^{0} (dW_n/dz)^3 dz}{\int_{-H}^{0} (dW_n/dz)^2 dz} \tag{11}$$

$$\beta_n = \frac{c_n}{2} \frac{\int_{-H}^{0} W_n^2 dz}{\int_{-H}^{0} (dW_n/dz)^2 dz} \tag{12}$$

If the shallow-water approximation holds, the analytical solution for the K-dV equation is a squared hyperbolic secant function: $\eta_n = \eta_{0,n} \operatorname{sech}^2((x - v_n t)/\Delta_n)$. Here,

$\eta_{0,n}$ is the amplitude, $v_n = c_n + (\alpha_n \eta_{0,n}/3)$ is the nonlinear phase speed, and $\Delta_n = \sqrt{12\beta_n/\alpha_n \eta_{0,n}}$ is the nonlinear characteristic width; $\eta_{0,n}$ or v_n increases when Δ_n decreases. The signs of α_n and $\eta_{0,n}$ are the same (Apel et al. 1997).

Consequently, amplitude (A_2), vertical (w_2) and horizontal (u_2) current velocity components, and the quadratic nonlinearity coefficient (α_2) can be calculated from Eqs. (3), (4), and (11) for a mode-2 ISW in this three-layer ocean model:

$$A_2(x,z,t) = \eta_2(x,t)W_2(z) = \eta_{0,2}W_2(z)\operatorname{sech}^2(\frac{x - v_2 t}{\Delta_2}) \tag{13}$$

$$w_2(x,z,t) = \frac{\partial A_2(x,z,t)}{\partial t} = \frac{2v_2}{\Delta_2}\eta_{0,2}W_2(z)\operatorname{sech}^2(\frac{x - v_2 t}{\Delta_2})\tanh(\frac{x - v_2 t}{\Delta_2}) \tag{14}$$

$$u_2(x,z,t) = -\int \frac{\partial w_2}{\partial z} dx = v_2 \eta_{0,2} U_2(z)\operatorname{sech}^2(\frac{x - v_2 t}{\Delta_2}) \tag{15}$$

$$\alpha_2 = \frac{3c_2}{2}\frac{\frac{\gamma_2^3}{h_3^2} + \frac{(1-\gamma_2)^3}{h_2^2} - \frac{1}{h_1^2}}{\frac{\gamma_2^2}{h_3} + \frac{(1-\gamma_2)^2}{h_2} + \frac{1}{h_1}} \tag{16}$$

By Eq. (16), the quadratic nonlinearity coefficient is not only a function of layered thickness but also of density difference. It is more complicated than the two-layer ocean model solution. Positive and negative $\eta_{0,2}$ values (or α_2) represent convex and concave waves, respectively.

Physically, each interface could have two degrees of freedom displacement so that a three-layer ocean (two interfaces) could have the following four types of ISWs: (1) in-phase motion in the upper and lower interfaces; both have upward and then downward interfacial displacement, which corresponds to the elevation type of mode-1 ISW; (2) in-phase motion of the upper and lower interfaces; both have downward and then interfacial upward displacement, which corresponds to the depression type of mode-1 ISW, (3) out-of-phase motion in upper and lower interfaces; the upper interface produces upward and then downward displacement and the lower interface evolves as downward and then upward displacement, which corresponds to the convex type of mode-2 ISW; and (4) out-of-phase motion in the upper and lower interfaces; if the upper interface produces downward and then upward displacement and the lower interface evolves as upward and then downward displacement, this corresponds to a concave type of mode-2 ISW. In summary, there are two vertical modes in the three-layer ocean model. Each ISW mode has two polarities: elevation and depression types for mode-1 ISW and convex and concave types for mode-2 ISW. The analytical results of the three-layer ocean model agree with the physical explanation.

The convex and concave wave solutions are discussed in the next section. Meanwhile, the mode-2 ISW polarity will be examined by changing the layer thickness and density.

4. Results

Two cases are examined for mode-2 ISW solutions. According to Eqs (5), (9), and (16), the solutions and polarity of mode-2 ISWs depend on the sign of α_2, which is a function of the thickness of the three layers (h_1, h_2, and h_3) and the density difference at the two interfaces ($\Delta\rho_1$ and $\Delta\rho_2$). In the first case, the stratification parameters are set to $h_1 = 0.3H$, $h_2 = 0.4H$, $h_3 = 0.3H$, and $\Delta\rho_1 = \Delta\rho_2$. The corresponding quadratic nonlinearity coefficient is $\alpha_2 = 2.5c_2/H$. This coefficient represents a convex wave, and the wave amplitude is set to $\eta_{0,2} = 0.1H$. The parameters for this case are summarized in Tab. 1.

Figure 5 shows the convex case solution, from left to right, which are amplitude and horizontal and vertical current components as a function of distance and depth, respectively. First, an elevation and a depression wave appear in the upper and lower water columns, respectively (Figs. 5a and 5c), which indicates that this wave is a convex type. Second, the middle layer current direction is consistent with the mode-2 ISW propagation direction (Fig. 5b). Therefore, we can use the current direction at the middle layer to determine the propagation direction of the convex wave. The solutions for this case are similar to the observation results shown in Fig. 2.

In the second case, the stratification parameters are set to $h_1 = 0.2H$, $h_2 = 0.6H$,

$h_3 = 0.2H$, and $\Delta\rho_1 = \Delta\rho_2$. The corresponding quadratic nonlinearity coefficient is $\alpha_2 = -2.5c_2/H$, which represents a concave wave, and the wave amplitude is set to $\eta_{0,2} = -0.1H$. The parameters of this case are summarized in Tab. 1.

Figure 6 shows the concave case solution, giving from left to right, the amplitude and the horizontal and vertical current components as a function of distance and depth, respectively. First, a depression and an elevation wave appear in the upper and lower water column, respectively (Figs. 6a and 6c), demonstrating that the wave behaves as a concave type. Second, the upper or lower layer current direction is the same as the wave propagation direction (Fig. 6b). Therefore, the propagation direction of a convex wave is determined by the upper or lower layer current direction, which is why we suggest that the concave wave shown in Fig. 3 is propagating to the west. The solutions for this case are different than those for the convex case but similar to the Fig. 3 observation results.

Figures 5 and 6 show that the mode-2 ISW polarity depends on the signs of $\eta_{0,2}$ (or α_2). The value of α_2 is a function of layer thickness (h_1, h_2, and h_3) and the density differences at the upper and lower interfaces ($\Delta\rho_1$ and $\Delta\rho_2$). Figure 7 shows positive α_2 (convex wave) and negative α_2 (concave wave) regions as a function of h_1 and h_2 when δ ($\Delta\rho_1/\Delta\rho_2$) was adjusted to 0.5, 1, and 2, respectively. Most of the region approaches a negative α_2 or a positive α_2 when the middle layer thickness h_2 becomes larger or smaller, respectively. Different δ values only slightly influence the patterns in Fig. 7. It follows that the transition of the mode-2 ISW polarity occurs when the middle layer is sufficiently thick or thin. Therefore, the three-layer ocean model implies that a thinner middle layer will be favorable for convex waves, whereas a thicker middle layer would accompany concave waves, which generally agrees with the observations. When $h_2/H > 0.5$, α_2 is always less than zero, meaning only concave waves are possible. Figures 2c and 3c show that the middle layer thickness (distance between the locus of local w' maximum and minimum) of the convex wave (120 m) was thinner than that of the concave wave (160 m).

According to the analytical solutions, the polarity of mode-2 ISWs is determined by the quadratic nonlinearity coefficient. In a three-layer ocean model, the density difference between the layers slightly influences the quadratic nonlinearity coefficient, and h_2 mainly affects mode-2 ISW polarity. If the middle layer thickness is larger than half the water column, the resulting mode-2 ISW waveform is always concave, regardless of the density difference at the two interfaces.

5. Discussion and summary

Previous studies have investigated the convex type wave because the initial condition was always based on an environment with a thin middle layer. Stratification with a "thick" middle layer as defined in Fig. 7 is rare over the continental slope and shelf, thus the concave wave is not commonly observed in the ocean and has not been considered in the laboratory. However, four examples of concave mode-2 ISWs have now been observed in the northern South China Sea during the VANS/WISE experiment. The three-layer thermal structure with a thick middle layer was sometimes observed over the continental slope and shelf of the northern South China Sea (Yang et al. 2004). This thermal structure allowed a concave wave to be generated, as suggested by the analytical model results.

When there was a thin middle layer, the two interfaces were relatively far from the rigid-lid boundary. Consequently, it was easier to allow an elevation and a depression wave (convex) to exist at the upper and lower interface, respectively. However, when there was a thick middle layer, the two interfaces were relatively close to the rigid-lid boundary. A depression and an elevation wave (concave) existed more easily at the upper and lower interface, respectively.

When the resulting mode-2 ISW propagated in the same direction as current in the upper and lower layers, by Eq. (15), a convergence zone ($\partial u/\partial x < 0$) and a divergence zone ($\partial u/\partial x > 0$) were produced in these two layers at the front and rear of the mode-2 ISW, respectively. Due to the rigid-lid boundary condition and volume conservation, the downwelling/upwelling processes had to occur in the upper layer at the front/rear of the wave. Similarly, upwelling/downwelling processes appeared in the lower layer. These processes correspond to a concave-shaped waveform. This result indicates that the concave wave propagated in the same direction as current in the upper and lower layers, respectively. On the other hand, when the resulting mode-2 ISW propagated in the same direction as current in the middle layer, a convergence and a divergence zone were also produced at the front and rear of the mode-2 ISW, respectively, in the middle layer. Consequently, upward/downward and downward/upward displacements were induced at the upper and lower interfaces, respectively, showing a convex wave with a propagation direction that is consistent with the current direction in the middle layer.

The upper layer circulation resembles a mode-1 depression wave for the concave case, and a mode-1 elevation wave for the convex case. This means that the surface signatures in the Synthetic Aperture Radar (SAR) imagery should resemble those waves, but likely weaker and more intermittent. The divergence ahead of the convex wave and convergence behind should product a dark/light pattern (smooth/rough) in the SAR imagery, and conversely for the concave wave (Alpers 1985; Liu et al. 1998; Chang et al. 2008). While mode-2 waves have been observed in the Moderate Resolution Imaging Spectroradiometer (MODIS) imagery (Yang et al., 2009) they have not yet been observed in the SAR imagery.

From the three-layer ocean model results, the turning point function ($\alpha_2 = 0$) is more complicated than that of the two-layer ocean model results. However, the mode-2 ISW polarities are dependent on layer thicknesses and the density difference at the two interfaces. In particular, the mode-2 ISW waveform is always the concave type as long as the middle layer thickness is larger than half of the water column. However, this is an analytical three-layer ocean model result, and thus further studies are needed, especially those that consider more complicated conditions, such as continuous stratification, full nonlinearity, and non-hydrostatic effects.

Using the VANS/WISE mooring observations for the continental slope of the northern South China Sea, data collected by the ADCP, the three RCM8s, and the 16 temperature sensors revealed a number of mode-2 ISW episodes. The mode-2 ISWs had convex-shaped and concave-shaped waveforms, and more convex-shaped episodes occurred than concave-shaped episodes. The vertical structures of mode-2 ISWs generally agreed with the linear modal functions. The maximum/minimum vertical current component loci were close to the nodal points of the horizontal current component. Convex and concave waves were accompanied by thinner and thicker middle layer, respectively. The mode-2 ISW propagation direction was the same as the current direction in the middle (upper or lower) layer for the convex (concave) wave. The analytical solutions generally agreed with the observations. The mode-2 ISW polarities are related to the sign of the quadratic nonlinearity coefficient of the K-dV equation. In the three-layer ocean model, the polarities were not only a function of the thickness of each layer but also related to the density difference at the two interfaces. A convex wave was found when there was a thin middle layer. When the middle layer thickness was larger than half the water column, the resulting mode-2 ISW was always concave shaped. Although mode-2 ISWs are not as energetic as mode-1 ISWs observed in the same region, they potentially play a significant role for mixing shelf waters (Moum et al. 2008). Future studies are needed to fully elucidate the nature of convex and concave waveforms.

Acknowledgments. This work was funded by the National Science Council, Taiwan (NSC 93-2611-M-002-019, 93-2611-M-012-001, 94-2611-M-002-003, and 94-2611-M-012-001), and the Office of Naval Research. We thank the technical support groups at National Taiwan University and the Naval Postgraduate School, who all worked tirelessly to execute the fieldwork at sea. We are also grateful to the captain and crew members of the *R/V Ocean Researcher I* for their contributions to the success of this experiment.

REFERENCES

Akylas, T., and R. Grimshaw, 1992: Solitary internal waves with oscillatory tails. *J. Fluid Mech.*, **242**, 279-298.

Alpers, W., 1985: Theory of radar imaging of internal waves, *Nature*, **314**, 245-247.

Antenucci, J. P., J. Imberger, and A. Saggio, 2000: Seasonal evolution of basin-scale internal wave field in a large stratified lake. *Limnol. Oceanogr.*, **45**, 1621-1638.

Apel, J. R., 2003: A new analytical model for internal solitons in the ocean. *J. Phys. Oceanogr.*, **33**, 2247-2269.

———, J. R., L. A. Ostrovsky, Y. A. Stepanyants, and J. F. Lynch, 2007: Internal solitons in the ocean and their effect on underwater sound. *J. Ascust. Soc. Am.*, **121**, 695-722.

———, M. Badiey, C.-S. Chiu, S. Finette, R. Headrick, J. Kemp, J. F. Lynch, A. Newhall, M. H. Orr, B. H. Pasewark, D. Tielbuerger, A. Turgut, K. von der Heydt, and S. Wolf, 1997: An overview of the 1995 SWARM Shallow-Water Internal Wave Acoustic Scattering Experiment. *IEEE J. Oceanic Eng.*, **22**, 465-500.

Benjamin, T. B., 1967: Internal waves of permanent form in fluids of great depth. *J. Fluid Mech.*, **29**, 559-592.

Benny, D. J., 1966: Long non-linear waves in fluid flow. *J. Math. Phys.*, **45**, 52-63.

Boegman, L., J. Imberger, G. N. Ivey, and J. P. Antenucci, 2003: High-frequency internal waves in large stratified lakes. *Limnol. Oceanogr.*, 48, 895-919.

Bogucki, D. J., L. G. Redekopp, and J. Barth, 2005: Internal solitary waves in the Coastal Mixing and Optics 1996 experiment: Multimodal structure and resuspension. *J. Geophys. Res.*, **110**, C02024, doi:10.1029/2003JC002253.

Chang, M.-H., R.-C. Lien, Y. J. Yang, T. Y. Tang, and J. Wang, 2008: A composite view of surface signatures and interior properties on nonlinear internal waves: Observations and applications. *J. Atmos. Oceanic Technol.*, **25**, 1218-1227.

Davis, R. E., and A. Acrivos, 1967: Solitary internal waves in deep water. *J. Fluid Mech.*, **29**, 593-607.

Duda, T. F., J. F. Lynch, J. D. Irish, R. C. Beardsley, S. R. Ramp, C.-S. Chiu, T. Y. Tang, and Y. J. Yang, 2004: Internal tide and nonlinear internal wave behavior at the continental slope in the northern South China Sea. *IEEE J. Oceanic Eng.*, **29**, 1105-1130

Farmer, D. M., and J. D. Smith, 1980: Tidal interaction of stratified flow with a sill in Knight Inlet. *Deep-Sea Res.*, **27A**, 239-254.

Gear, J., and R. Grimshaw, 1983: A second-order theory for solitary waves in shallow fluids. *Phys. Fluids*, **26**, 14-29.

Gill, A. E., 1982: *Atmosphere-Ocean Dynamics*. Academic Press, 662 pp.

Grimshaw, R., 1981: Evolution equations for long nonlinear waves in stratified shear flow. *Stud. Appl. Math.*, **65**, 159-188.

———, E. Pelinovsky, and T. Talipova, 1997: The modified Kortewege-de Vries equation in the theory of large-amplitude internal waves. *Nonlinear Processes in Geophysics*, **4**, 237-250.

Helfrich, K. R., and W. K. Melville, 2006: Long nonlinear internal waves. *Ann. Rev. Fluid Mech.*, *38*, 395-425.

Honji, H., N. Matsunaga, Y. Sugihara, and K. Sakai, 1995: Experimental observation of internal symmetric solitary waves in a two-layer fluid. *Fluid Dyn. Res.*, **15**, 89-102.

Kao, T. W., and H.-P. Pao, 1980: Wake collapse in the thermocline and internal solitary waves. *J. Fluid Mech.*, **97**, 115-127.

Konyaev, K. V., K. D. Sabinin, and A. N. Serebryany, 1995: Large-amplitude internal waves at the Mascarene Ridge in the Indian Ocean. *Deep-Sea Res. I*, **42**, 2075-2091.

Korteweg, D. J., and G. de Vries, 1895: On the change of form of long waves advancing in a rectangular canal and on a new type of long stationary waves. *Phil. Mag.*, **39**, 422-443.

Lee, C.-Y., and R. C. Beardsley, 1974: The generation of long nonlinear internal waves in a weakly stratified shear flow. *J. Geophys. Res.*, **79**, 453-462.

Liu, A. K., Y. S. Chang, M.-K. Hsu, and N. K. Liang, 1998: Evolution of nonlinear internal waves in the East and South China Seas, *J. Geophys. Res.*, **103**, 7995-8008.

Maslowe, S. A., and L.G. Redekopp, 1980: Long nonlinear waves in stratified shear flows. *J. Fluid Mech.*, **101**, 321-348.

Maxworthy, T., 1980: On the formation of nonlinear internal waves from the gravitational collapse of mixed regions in two and three dimensions. *J. Fluid Mech.*, **96**, 47-64.

Mehta, A. P., B. R. Sutherland, and P. J. Kyba, 2002: Interfacial gravity currents. II. Wave excitation. *Phys. Fluids*, **14**, 3558-3569.

Moum, J. N., J. D. Nash, and J. M. Klymak, 2008: Small-scale processes in the coastal ocean. *Oceanography*, **21**, 22-33.

Ostrovsky, L. A., and Y. A. Stepanyants, 2005: Internal solitons in laboratory experiments: Comparison with theoretical modes. *Chaos*, **15**, 037111, 1-28.

Pelinovsky, E. N., and S. K. Shavratsky, 1977: Disintegration of cnoidal internal waves in a horizontally inhomogeneous ocean. *Atmos. Oceaic Phys.*, **13**, 455-456.

Ramp, R. R., Y. J. Yang, and F. L. Bahr, 2010: Characterizing the nonlinear internal wave climate in the northeastern South China Sea. *Nonlin. Processes Geophys.*, submitted.

Rubino, A., P. Brandt, and R. Weigle, 2001: On the dynamics of internal waves in a nonlinear, weakly nonhydrostatic three-layer ocean. *J. Geophys. Res.*, **106**, 26,899-26,915.

Rusås, P.-O., and J. Grue, 2002: Solitary waves and conjugate flows in a three-layer fluid. *Eur. J. Mech. B/Fluids*, **21**, 185-206.

Sabinin, K., and A. Serebryany, 2005: Intense short-period internal waves in the ocean. *J. Mar. Res.*, **63**, 227-261.

Saggio, A., and J. Imberger, 1998: Internal wave weather in a stratified lake. *Limnol. Oceanogr.*, **43**, 1780-1798.

———, and ———, 2001: Mixing and turbulent fluxes in a metalimnion of a stratified lake. *Limnol. Oceanogr.*, **46**, 392-409.

Shroyer, E. L., J. N. Moum, and J. D. Nash, 2010: Mode-2 waves on the continental shelf: ephemeral components of the nonlinear internal wave field. *J. Geophys. Res.*, in press.

Stamp, A. P., and M. Jacka, 1995: Deep-water internal solitary waves. *J. Fluid Mech.*, **305**, 347-371.

Stastna, M., and W. Peltier, 2005: On the resonant generation of large-amplitude internal solitary waves and solitary-like waves. *J. Fluid Mech.*, **543**, 267-292.

Sutherland, B. R., 2002: Interfacial gravity currents. I. Mixing and entrainment. *Phys. Fluids*, **14**, 2244-2254.

Terez, D. E., and O. M. Knio, 1998: Numerical simulations of large-amplitude internal solitary waves. *J. Fluid Mech.*, **362**, 53-82.

Tung, K.-K., T. F. Chan, and T. Kubota, 1982: Large amplitude internal waves of permanent form. *Stud. Appl. Math.*, **66**, 1-44.

Vlasenko, V. I., 1994: Multimodal soliton of internal waves. *Izv. Atmos. Oceanic Phys.*, **30**, 161-169.

———, and K. Hutter, 2001: Generation of second mode solitary waves by the interaction of a first mode soliton with a sill. *Nonlin. Proce. Geophys.*, **8**, 223-239.

———, and W. Alpers, 2005: Generation of secondary internal waves by the interaction of an internal solitary wave with an underwater bank. *J. Geophys. Res.*, **110**, C02019, doi:10.1029/2004JC002467.

Yang, Y. J., T. Y. Tang, M.-H. Chang, A. K. Liu, M.-K. Hsu, and S. R. Ramp, 2004: Solitons northeast of Tung-Sha Island during the ASIAEX pilot studies. *IEEE J. Oceanic Eng.*, **29**, 1182-1199.

———, Y. C. Fang, M.-H. Chang. S. R. Ramp, C.-C. Kao, and T. Y. Tang, 2009: Observations of second baroclinic mode internal solitary waves on the continental slope of the northern South China Sea. *J. Geophys. Res.*, **114**, C10003, doi:10.1029/2009JC005305.

Yih, C.-S., 1960: Gravity waves in a stratified fluid. *J. Fluid Mech.*, **8**, 481-508.

TABLE LISTS

FIGURE CAPTIONS

FIG. 1. The mooring location (shown as a red dot) on the continental slope of the northern South China Sea. The local depth was 350 m.

FIG. 2. The left (a), middle (b), and right (c) panels represent the contours of isotherms, perturbations of the eastward current component (u'), and vertical current component (w') as functions of time and depth, respectively, from 23:20 to 24:00 GMT 27 June 2005. The temperature data were measured by 16 temperature sensors at depths from 32 to 338 m. The eastward current data were measured by an ADCP between 15 and 95 m and three RCM8s at 160, 220, and 310 m. The contour intervals are 1°C, 10 cm s^{-1}, and 4 cm s^{-1} for temperature, u', and w', respectively. Positive u', and w' indicate eastward and upward velocities, respectively.

FIG. 3. Same as Fig. 2 except from 22:40 to 23:20 GMT 9 July 2005.

FIG. 4. The left (a), middle (b), and right (c) panels represent the mode-2 ISW vertical density profile (ρ) and vertical structure functions of horizontal (U_2) and vertical (W_2) current components, respectively, in the three-layer rigid-lid ocean.

FIG. 5. The left (a), middle (b), and right (c) panels represent the contours of amplitude (A_2) and horizontal (u_2) and vertical (w_2) current components for a convex mode-2 ISW as functions of distance and depth, respectively. The left panel also

displays A_2 at the upper and lower interfaces. All components were nondimensionalized using a horizontal length scale Δ_2 (nonlinear characteristic width of a mode-2 ISW), a vertical length scale H (depth), and a speed scale c_2 (linear phase speed of a mode-2 ISW). Shaded areas show negative values. The contour intervals are 0.02, 0.1, and 0.05 for A_2, u_2, and w_2, respectively.

FIG. 6. Same as Fig. 5, except for a concave mode-2 ISW.

FIG. 7. The solution space for the quadratic nonlinearity coefficient as a function of layer thickness and stratification. The axes have been nondimensionalized by the vertical length scale H (depth). The impact of changing stratification is shown by plotting the graphs for different values of the stratification parameter $\delta = \Delta\rho_1/\Delta\rho_2$ = 0.5, 1.0, and 2.0, for panels (a), (b), and (c) respectively. Shaded areas show negative values. The dashed lines represent the envelope when $\alpha_2 = 0$.

TAB. 1. The parameters for the two analytical three-layer ocean model cases.

Case	h_1	h_2	h_3	$\delta = \Delta\rho_1/\Delta\rho_2$	α_2	$\eta_{0,2}$	Waveform
I	$0.3H$	$0.4H$	$0.3H$	1	$2.5c_2/H$	$0.1H$	Convex
II	$0.2H$	$0.6H$	$0.2H$	1	$-2.5c_2/H$	$-0.1H$	Concave

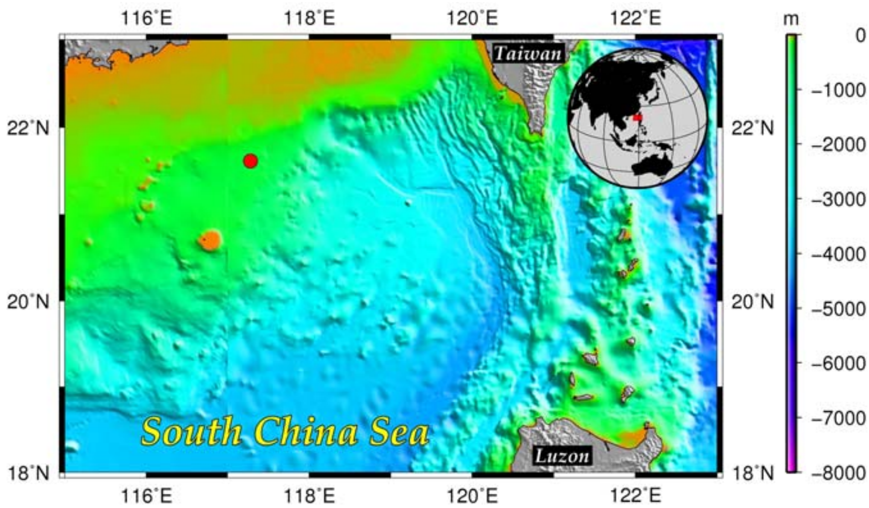

FIG. 1. The mooring location (shown as a red dot) on the continental slope of the northern South China Sea. The local depth was 350 m.

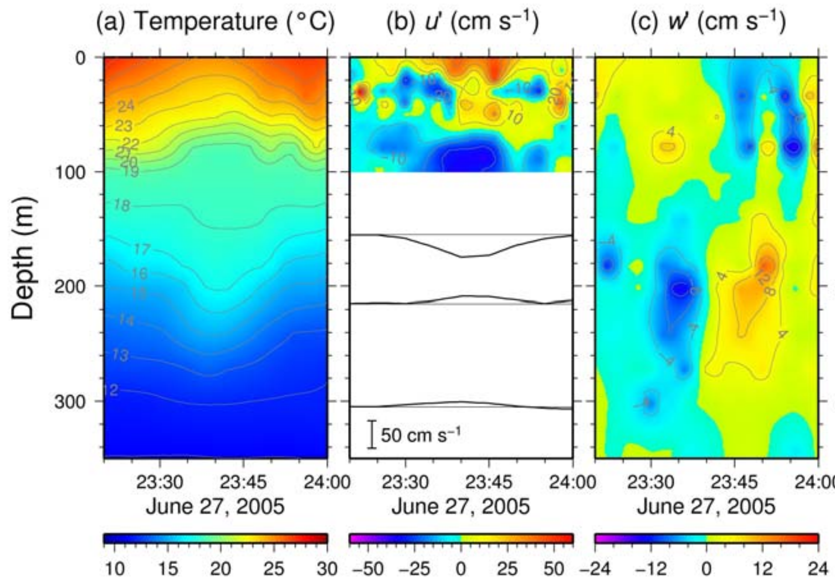

FIG. 2. The left (a), middle (b), and right (c) panels represent the contours of isotherms, perturbations of the eastward current component (u'), and vertical current component (w') as functions of time and depth, respectively, from 23:20 to 24:00 GMT 27 June 2005. The temperature data were measured by 16 temperature sensors at depths from 32 to 338 m. The eastward current data were measured by an ADCP between 15 and 95 m and three RCM8s at 160, 220, and 310 m. The contour intervals are 1°C, 10 cm s^{-1}, and 4 cm s^{-1} for temperature, u', and w', respectively. Positive u', and w' indicate eastward and upward velocities, respectively.

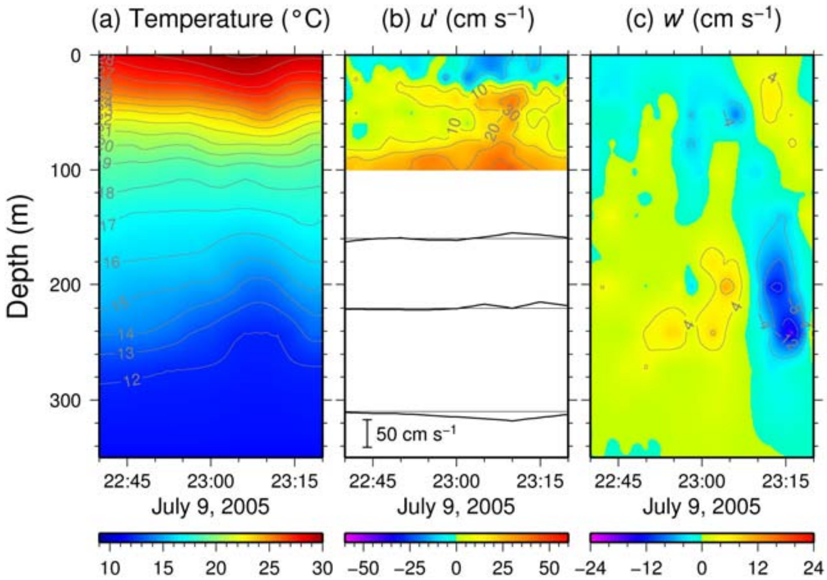

FIG. 3. Same as Fig. 2 except from 22:40 to 23:20 GMT 9 July 2005.

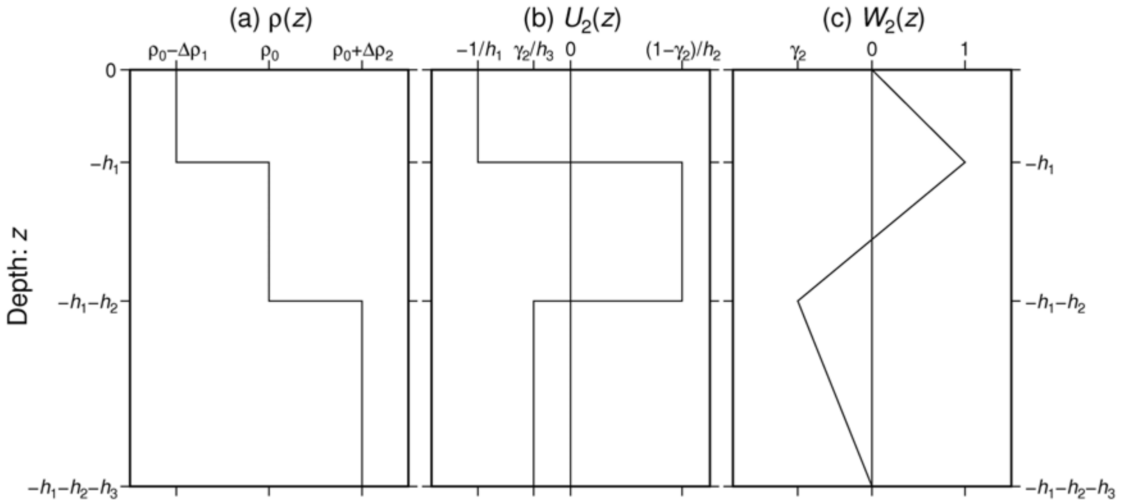

FIG. 4. The left (a), middle (b), and right (c) panels represent the mode-2 ISW vertical density profile (ρ) and vertical structure functions of horizontal (U_2) and vertical (W_2) current components, respectively, in the three-layer rigid-lid ocean.

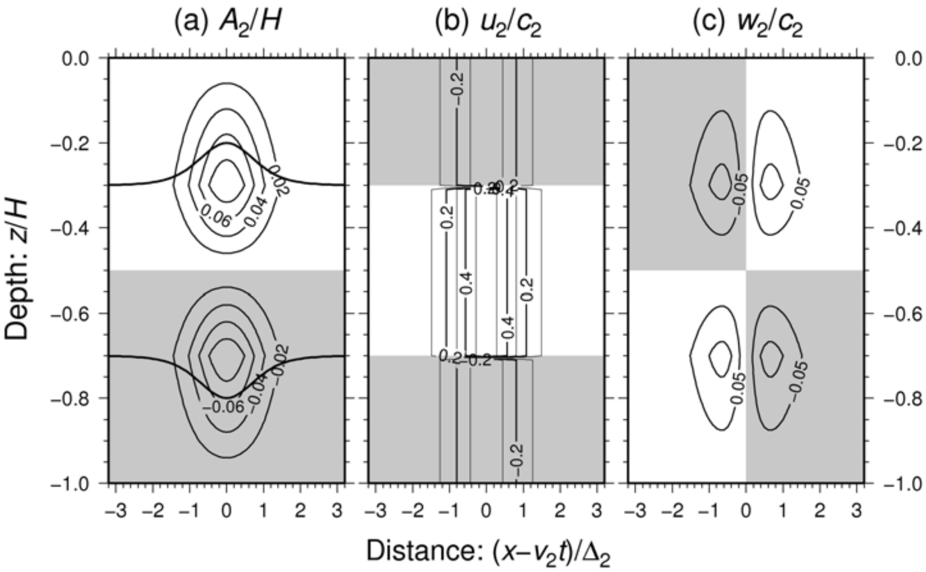

FIG. 5. The left (a), middle (b), and right (c) panels represent the contours of amplitude (A_2) and horizontal (u_2) and vertical (w_2) current components for a convex mode-2 ISW as functions of distance and depth, respectively. The left panel also displays A_2 at the upper and lower interfaces. All components were nondimensionalized using a horizontal length scale Δ_2 (nonlinear characteristic width of a mode-2 ISW), a vertical length scale H (depth), and a speed scale c_2 (linear phase speed of a mode-2 ISW). Shaded areas show negative values. The contour intervals are 0.02, 0.1, and 0.05 for A_2, u_2, and w_2, respectively.

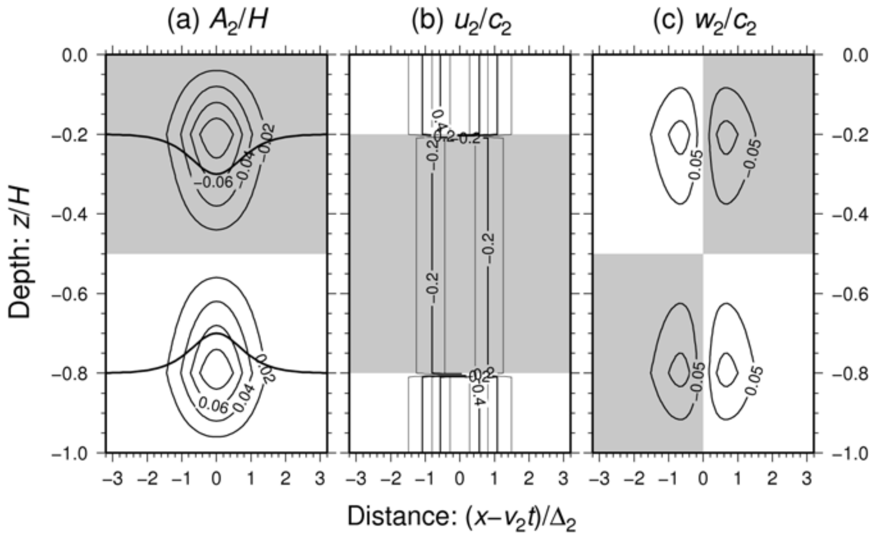

FIG. 6. Same as Fig. 5, except for a concave mode-2 ISW.

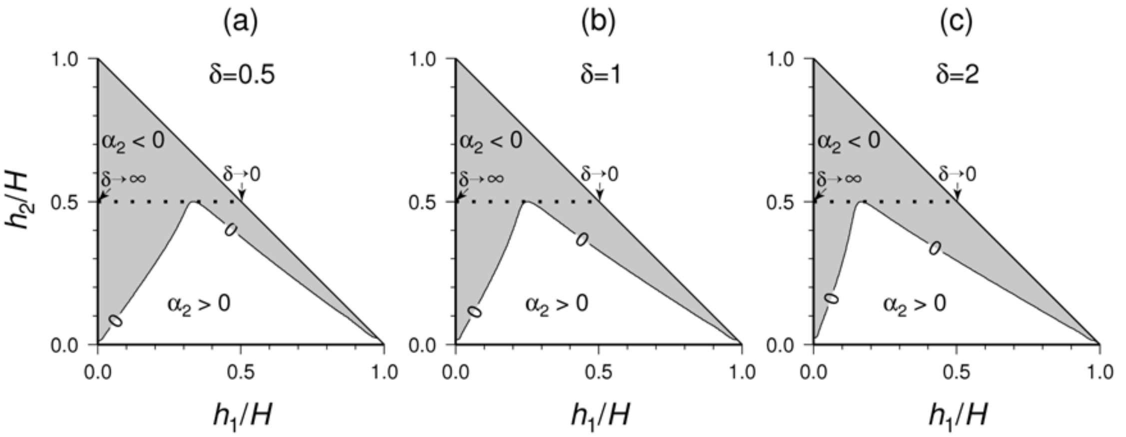

FIG. 7. The solution space for the quadratic nonlinearity coefficient as a function of layer thickness and stratification. The axes have been nondimensionalized by the vertical length scale H (depth). The impact of changing stratification is shown by plotting the graphs for different values of the stratification parameter $\delta = \Delta\rho_1/\Delta\rho_2$ = 0.5, 1.0, and 2.0, for panels (a), (b), and (c) respectively. Shaded areas show negative values. The dashed lines represent the envelope when $\alpha_2 = 0$.

附錄二：與會照片

主持人攝於研討會會場入口

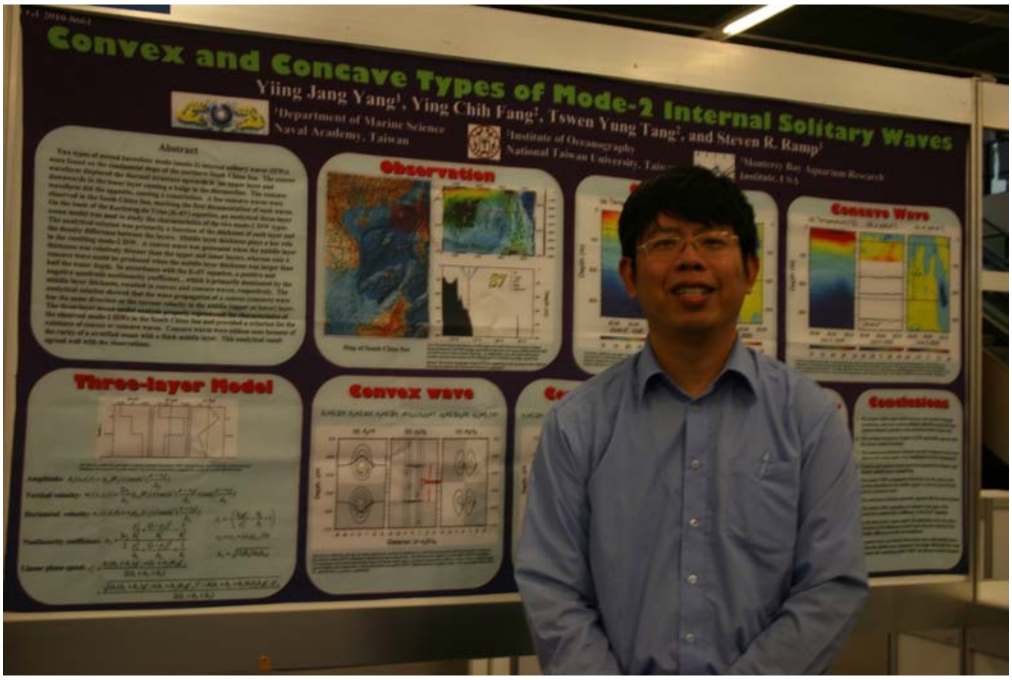

主持人攝於論文海報張貼處